Supporting Information

Co-MOF-derived carbon nanomaterials with size-controlled FeCo alloys for oxygen evolution

Junliang Chen,[a] Yunan Ye,[a] Yi Wu,[a] Jie Liu,[a] Xuemei Zhou,[a] Qipeng Li,[b] and Jinjie Qian*

[a]Key Laboratory of Carbon Materials of Zhejiang Province, College of Chemistry and Materials Engineering, Wenzhou University, Wenzhou 325035, Zhejiang, P. R. China

[b]College of Chemistry and Chemical Engineering, Zhaotong University, Zhaotong 657000, Yunnan, P. R. China

*Corresponding author

E-mail: jinjieqian@wzu.edu.cn (J. Qian)

Experimental section

Chemicals and Reagents

All chemicals are purchased and used without further purification. Cobalt(II) acetate tetrahydrate ($Co(CH_3COO)_2 \cdot 4H_2O$, AR), N-Methylformamide (NMF, 99%), Polyvinyl pyrrolidone (PVP, Mn= 58000), nitric acid concentrated solution (HNO_3, 70%), Ferric chloride ($FeCl_3$, AR), Urea (99%, AR) and ethanol (EtOH, moisture content ≤0.3% and ≤0.1%) are purchased from Shanghai Aladdin Corporation. Biphenyl-3,3',5,5'-tetracarboxylic acid (H_4BPTC, 98.0%, Jinan Henghua Technology Company), 5 wt% Nafion ionomers are purchased from Aldrich. All the salts, solvents and other reagents are of analytical grade. High-purity N_2, Ar gases, and deionized water (18.2 MΩ) are used in all experiments.

Synthesis of CoOF-1

$Co(CH_3COO)_2 \cdot 4H_2O$ (60 mg), H_4BPTC (30 mg), NMF (4 mL), EtOH (2 mL), PVP (400 mg), and HNO_3 (0.5 mL) are added to a 35 mL stress-tolerant glass tube. Then the pressure tube is placed into an aluminum model holding at 140 ℃ for 4 hours. The crystals of CoOF-1 are obtained by further washing with ethanol for 3 times.

Synthesis of CoOF-1-CoC

The obtained CoOF-1 is weighed and placed in the a CVD tube furnace for the following thermal treatment. The temperature is set to 900 ℃ at a heating rate of 10 ℃ min^{-1} under an Ar (50 sccm) atmosphere, and it is maintained at a constant temperature for another 2 hours. The black powders are obtained after falling to room temperature, denoted as CoOF-1-CoC (abbreviated as CoC).

Synthesis of CoOF-1-FeCoC-5/10/15

Three parts of obtained CoC (20 mg) are first dispersed in 5 mL deionized water and form homogeneous suspension. Then, 25/50/75 mg $FeCl_3$ (5/10/15 mg mL^{-1}) are added in the above suspension respectively and keep stirring for 30 min. Subsequently, the black powders are collected with centrifugation and followed by annealing at 900 ℃ and a heating rate of 10 ℃ min^{-1} under an Ar (50 sccm) atmosphere for 2 hours. The materials are obtained after falling to room temperature, denoted as CoOF-1-FeCoC-5/10/15 (abbreviated as FeCoC-5/10/15).

Synthesis of CoOF-1-FeCoNC-CNT-5/10/15

Three parts of obtained CoC (20 mg) are first dispersed in 5 mL deionized water and form homogeneous suspension. Then, 25/50/75 mg $FeCl_3$. (5/10/15 mg mL^{-1}) are added in the above suspension respectively and keep

stirring for 30 min. Subsequently, the black powders are collected with centrifugation and placed in a CVD tube furnace with urea (fivefold weight of the black powders) for the following thermal treatment. The temperature is set to 800 ℃ at a heating rate of 10 ℃ min^{-1} under an Ar (50 sccm) atmosphere, and it is maintained at a constant temperature for another 2 hours. The materials are obtained after falling to room temperature, denoted as CoOF-1-FeCoNC-CNT-5/10/15 (abbreviated as FeCoNC-CNT-5/10/15 or FeCoNC-5/10/15).

Material Characterization

The morphology of the samples is analyzed using a Nova NanoSEM 200 scanning electron microscope (FE-SEM, FEI Inc.). N_2 adsorption study is measured in the Specific Surface Area & Pore Size Analyzer (BSD-PS1, Beishide Instrument Technology (Beijing) Co., Ltd.)), where the samples after the activation of the high temperatures are placed in a clean ultra-high vacuum system and the cryogenic temperature of 77 K. The structure and properties are characterized using transmission electron microscopy (TEM, JEOL JEM-2100F microscope), as well as the high-resolution transmission electron microscope (HR-TEM) image and energy Dispersive X-ray spectroscopy (EDS) pattern. Powder X-ray diffraction (PXRD) maps of the products were acquired on a Bruker (Karlsruhe, Germany) D8 Advance powder diffractometer at room temperature, operating at 40 kV, 40 mA,

graphite monochromated Cu K_α radiation (λ = 1.54 Å). X-ray photoelectron spectroscopy (XPS) is conducted on PHI 5000 VersaProbe III. Raman spectrometer (LabRAM HR Evolution) is used to investigate the phase composition of samples at GS1000. Thermal gravimetric analysis (TGA) is performed on a NETZSCH STA 449C instrument where pure nitrogen as a carrier gas with a heating rate of 10 ℃ min^{-1}.

Electrochemical measurements

The applied potentials were calibrated to the reversible hydrogen electrode (RHE), unless otherwise mentioned. The electrochemical experiments are carried out at room temperature using a CHI 760E electrochemical station for OER. The experiment used the electrodes of Hg/HgO and platinum net are sequentially behaved as the reference (RE) and counter electrodes (CE), which are used in 1.0 M KOH electrolyte solution. According to a formula ERHE = ESCE + 0.098 V + 0.059 V × pH = ESCE + 0.912, all of its potentials can be corrected to reversible hydrogen electrode (RHE) potentials. The catalyst powder (5 mg) is dispersed in a mixture solution of 500 μL (300 μL EtOH, 150 μL deionized water, and 50 μL 5 wt % Nafion solution) and ultrasonicated for 2 h to form a homogeneous catalyst ink. Thereafter, the surface of glassy carbon (diameter: 3 mm) is loaded with 5 μL of a catalyst ink, wherein 0.7 mg cm^{-2} is calculated the loading amount. Linear sweep voltammetry (LSV) is conducted in electrolyte solution with

95% iR correction (a scan rate: 5 mV s^{-1}). The Tafel slope is transferred according to Tafel equation as follows: $\eta = b \times \log (j / j0)$. Regarding the evaluation of the electrochemical active surface areas (ECSA) of the samples, CV has also been performed by measuring the double-layer capacitances (C_{dl}) with various scan rate (20, 40, 60, 80, 100 and 120 mV s^{-1}) under the potential window of 1.012-1.062 V vs. RHE. The Nyquist plots of EIS are collected from 106 Hz to 0.01 Hz with an amplitude of 5 mV at 1.55 V vs. RHE in 1 M KOH. For evaluating the long-term performance, the electrochemical stability of the FeCoNC-CNT and RuO2 are conducted at a constant current density of 10 mA cm^{-2} for achieving a high initial potentials. In order to calculate the electron transfer number (N), rotating ring-disk electrode (RRDE) voltammogram of as-prepared samples are conducted to collect disk current (Idisk) and ring current (Iring) at the same time, equation as follows: $N=4 \times Id / (Id + Ir / Nc)$, where Ir is the ring current, Id is the disk current, and Nc is the current collection efficiency. The Faradaic efficiency (ε) is calculated by the equation as follows: $\varepsilon = Ir /(Id \cdot Nc)$.

Discussion of Fe^{3+} etching process

The feasibility of Fe^{3+} etching was displayed as followed.

Firstly, according to previous work, the relative standard electrode potential was listed below:

$$Fe^{2+} + 2e^- \leftrightarrow Fe\ (s) \qquad E^{\ominus}_{1} = -0.44\ V \qquad (1)$$

$$Fe^{3+} + 3e^- \leftrightarrow Fe\ (s) \qquad E^{\ominus}_{2} = -0.04\ V \qquad (2)$$

$$Co^{2+} + 2e^- \leftrightarrow Co\ (s) \qquad E^{\ominus}_{3} = -0.28\ V \qquad (3)$$

Therefore, the reaction between Co nanoparticles and Fe^{3+} can be integrated as followed:

$$Co\ (s) + 2Fe^{3+} \leftrightarrow Co^{2+} + 2Fe^{2+} \qquad E^{\ominus}_{4} = 1.08\ V \qquad (4)$$

According to Nernst equation: $\Delta G^{\ominus} = -zFE^{\ominus}$ (Where the $\Delta G^{\ominus}$, z, F, and $E^{\ominus}$ stand for the standard Gibbs free energy, electron transfer number, Faraday constant, and the standard electrode potential, respectively), the $\Delta G^{\ominus}_{4}$ is calculated to < 0, which means the reaction is theoretically spontaneous.

Moreover, the CoC samples were immersed in deionized water and $FeCl_3$ solution for 0.5 h respectively and the image was depicted below:

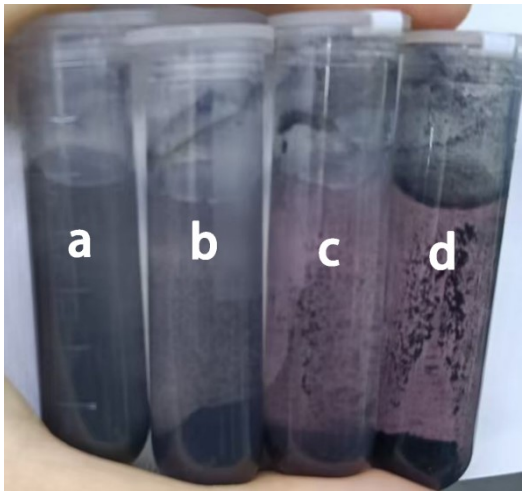

Figure S1. The image of the CoC samples immersed in deionized water and $FeCl_3$ solution for 0.5 h. (a: deionized water; b-d: $FeCl_3$ solution, where the concentration are 5, 10, 15 mg mL^{-1}, respectively.)

As shown in **Figure S1**, the solution in (a) displayed no obvious change, while the color of the solution in (b-d) turned pink (formation of Co^{2+}), which meant the successful reaction between Co nanoparticles and Fe^{3+}. Additionally, the color became denser as the concentration of Fe^{3+} increased, which was attributed to the further etching of Co.

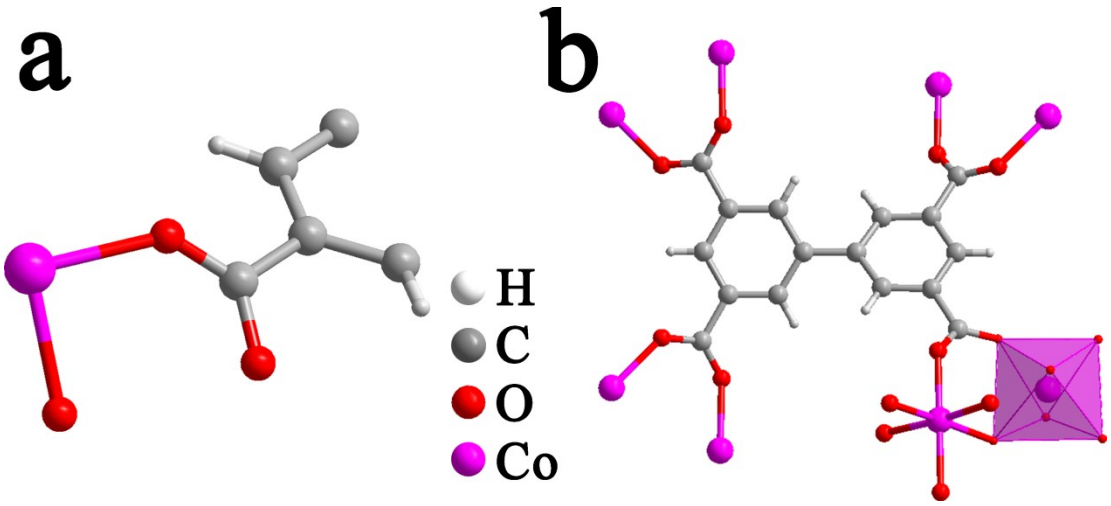

Figure S2. (a) The asymmetric unit of CoOF-1. (b) Coordination environment of the $BPTC^{4-}$ ligand and the 6-coordinated octahedron geometry of Co(II) center in CoOF-1.

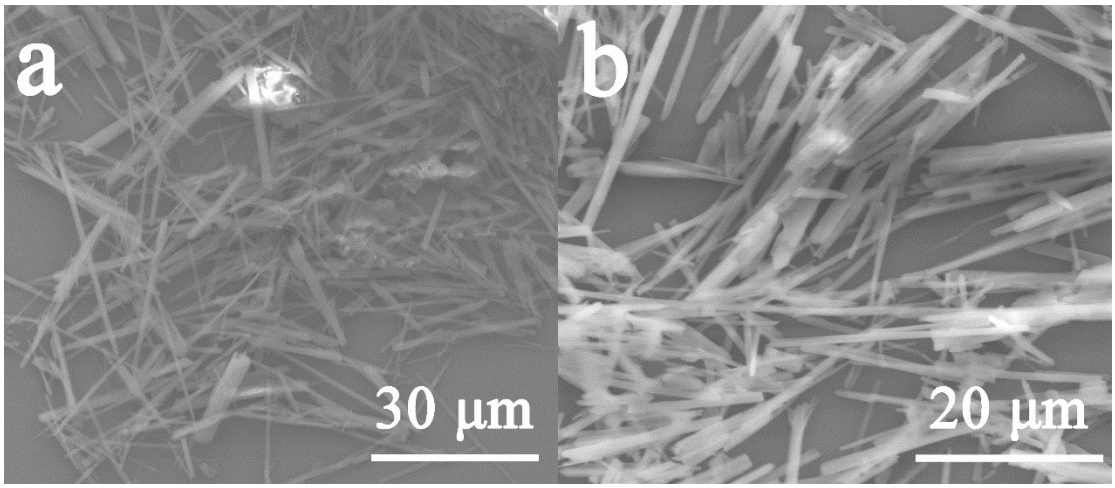

Figure S3. The SEM images of CoOF-1.

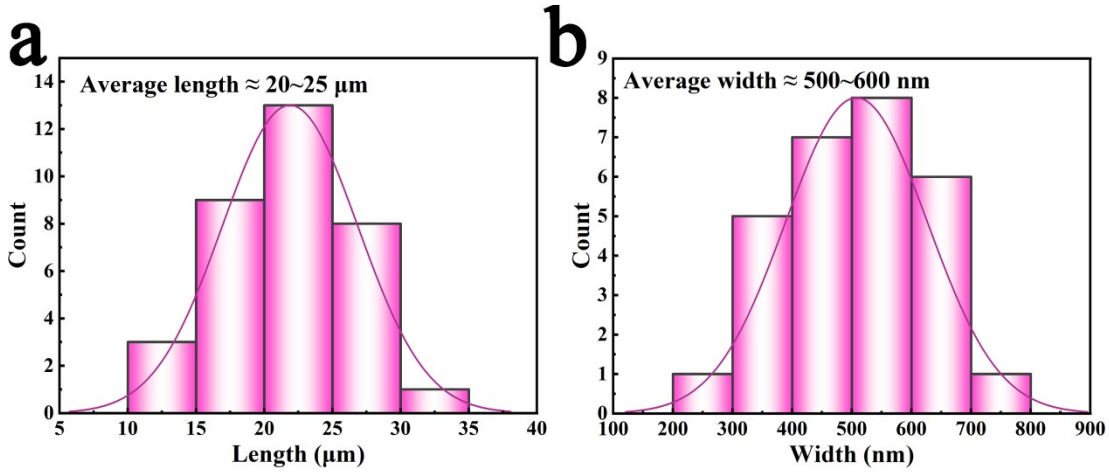

Figure S4. (a) Length and (b) width distribution of CoOF-1.

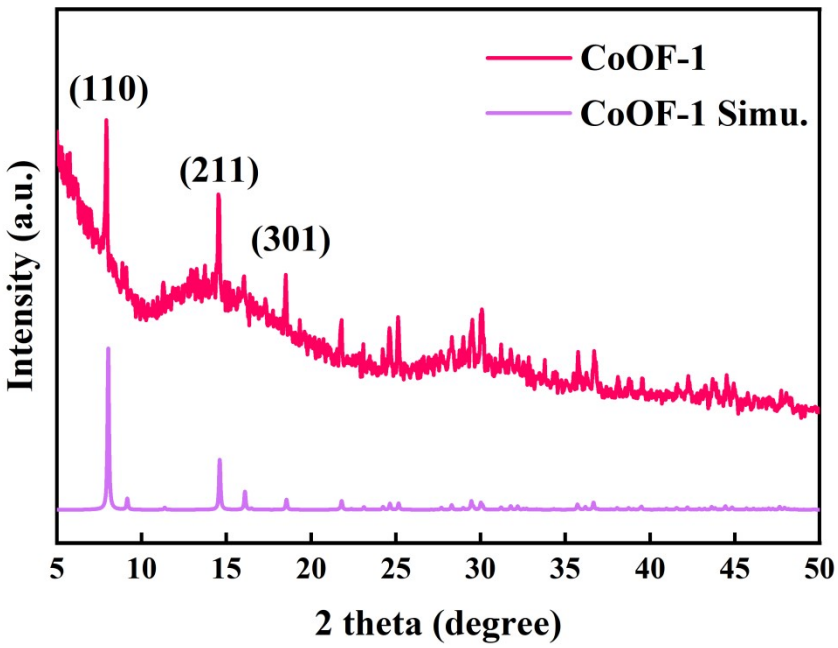

Figure S5. The PXRD analysis of CoOF-1.

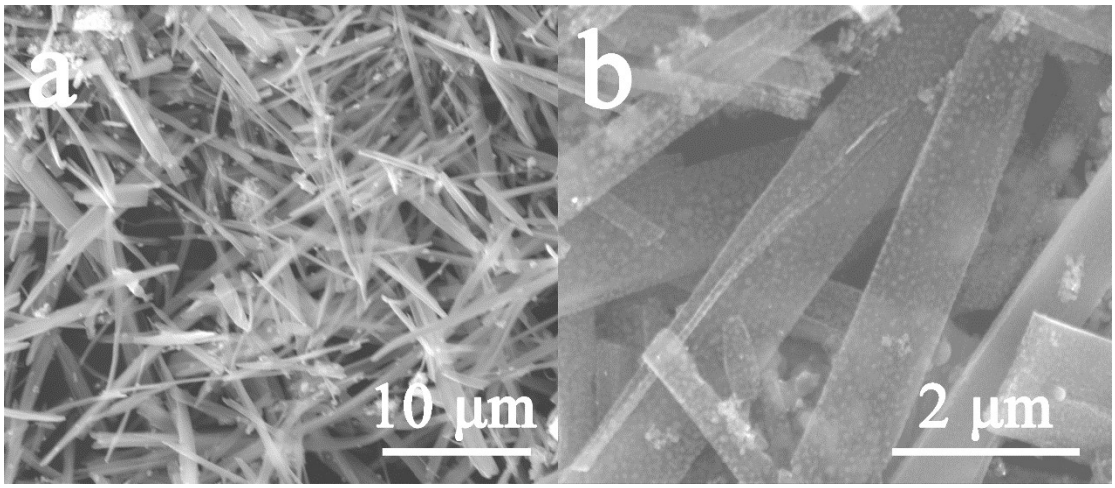

Figure S6. The SEM images of CoC.

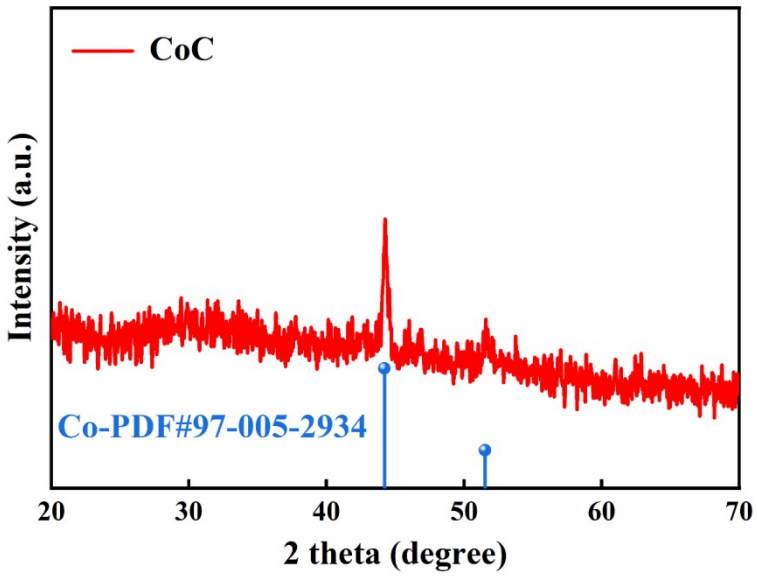

Figure S7. The PXRD analysis of CoC.

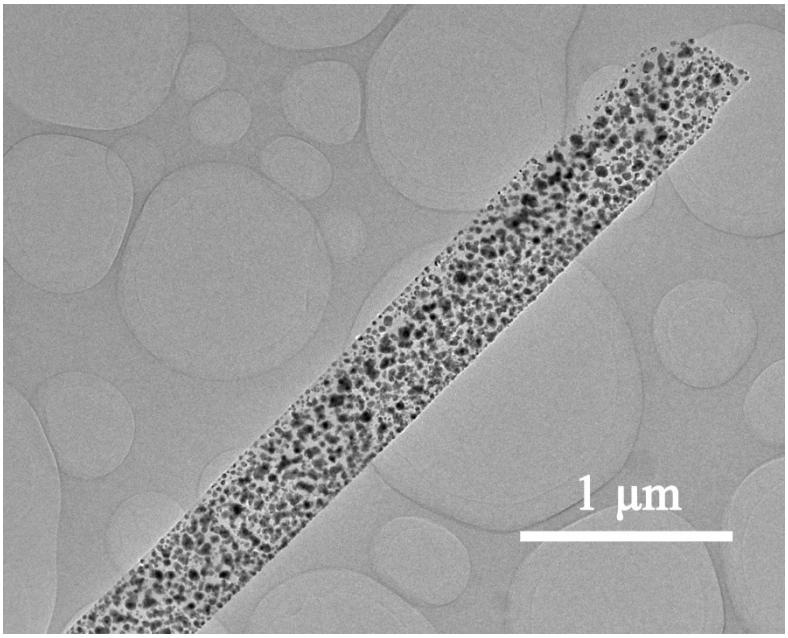

Figure S8. The TEM image of CoC.

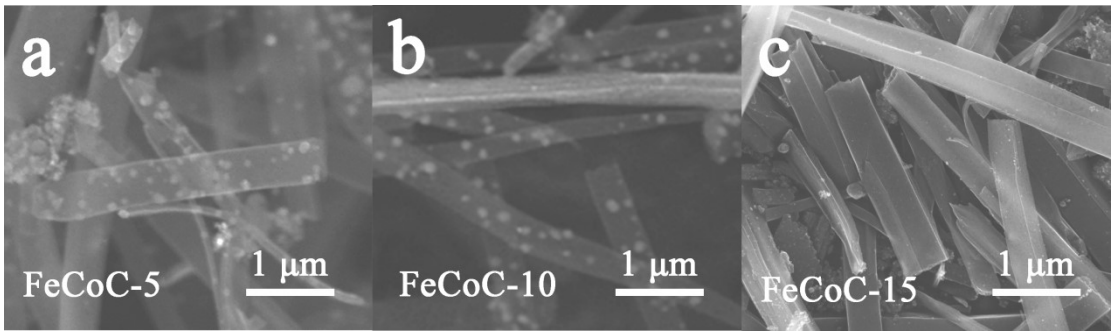

Figure S9. The magnified SEM images of FeCoC series.

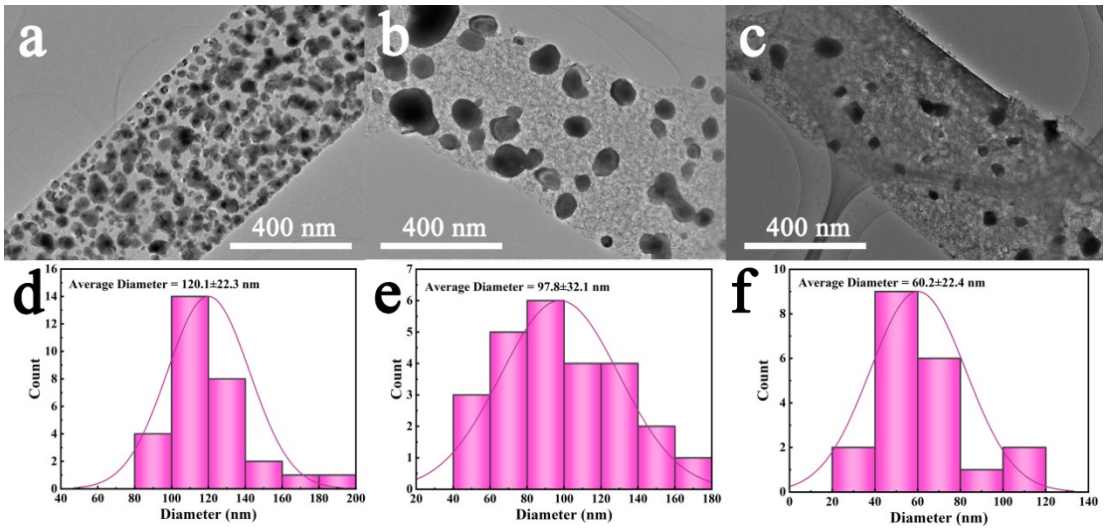

Figure S10. (a-c) The TEM images of CoC, FeCoC-5/10, respectively. And (d-f) the particles diameter statistics of CoC, FeCoC-5/10, respectively.

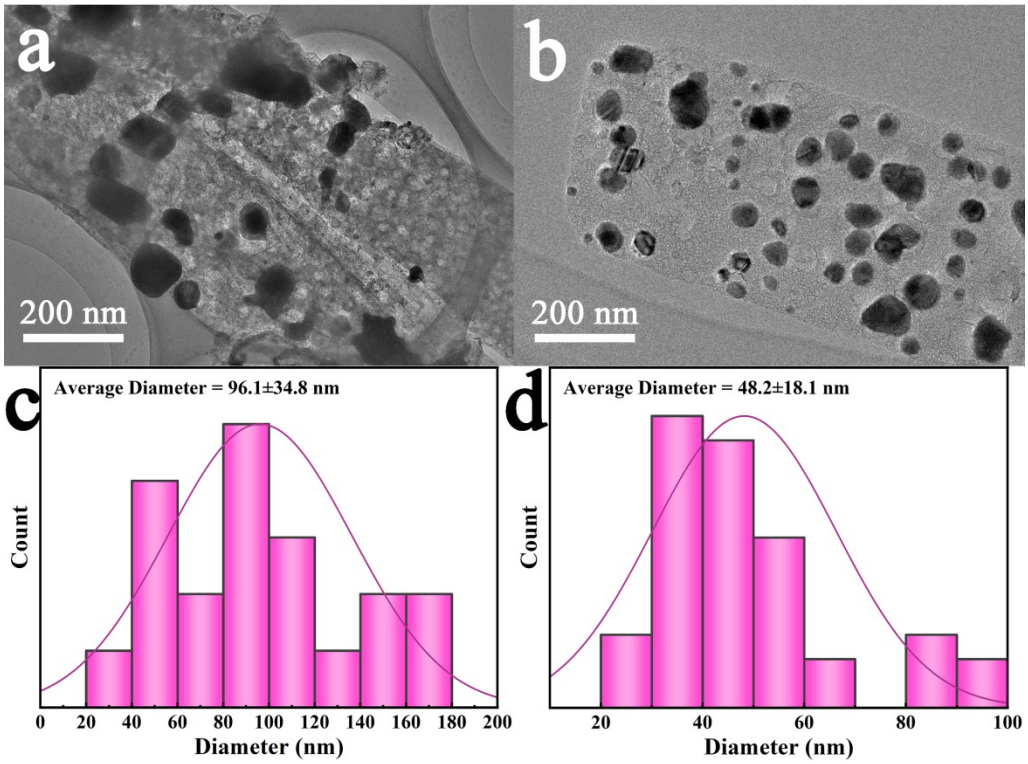

Figure S11. (a-b) The TEM images of FeCoNC-5/10, (c-d) the particles diameter statistics of FeCoNC-5/10.

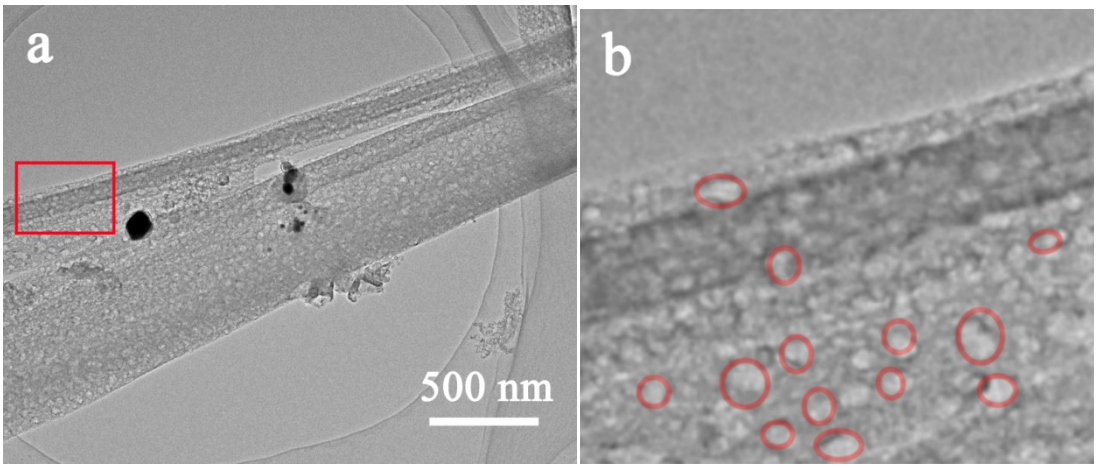

Figure S12. The TEM image (a) and its highlighted zone (b) of FeCoNC-CNT-15 with visible porous structure.

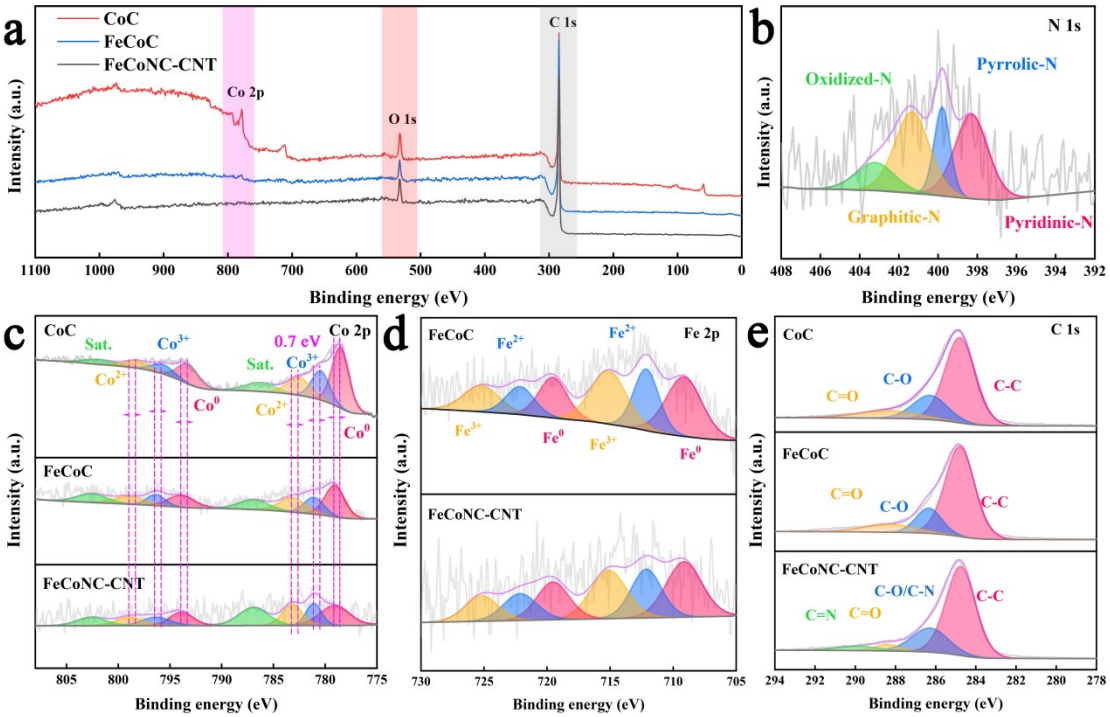

Figure S13. The XPS full spectra of CoC (red), FeCoC (blue), and FeCoNC-CNT (grey). The deconvoluted XPS spectra of (b) N 1s, (c) Co 2p, (d) Fe 2p, and (e) C 1s for these MOF-derived carbon nanomaterials.

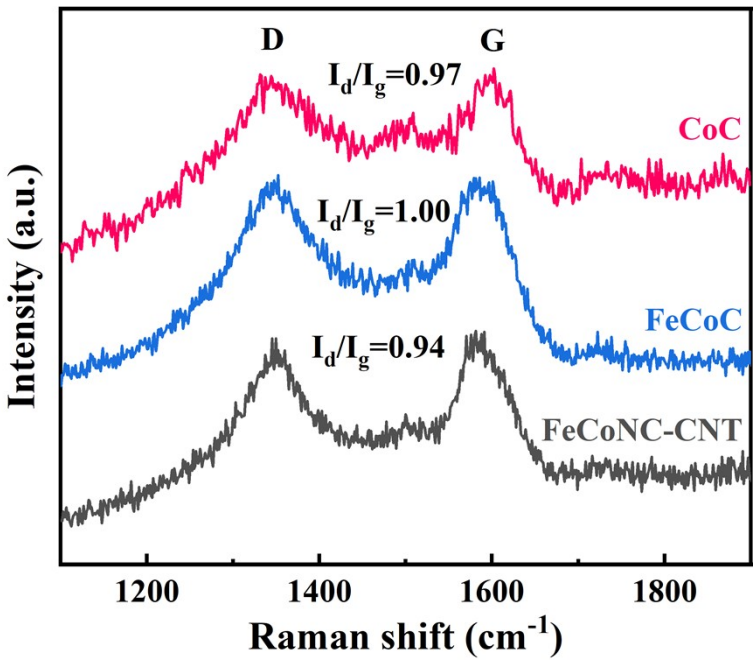

Figure S14. The Raman spectra of CoC, FeCoC and FeCoNC-CNT.

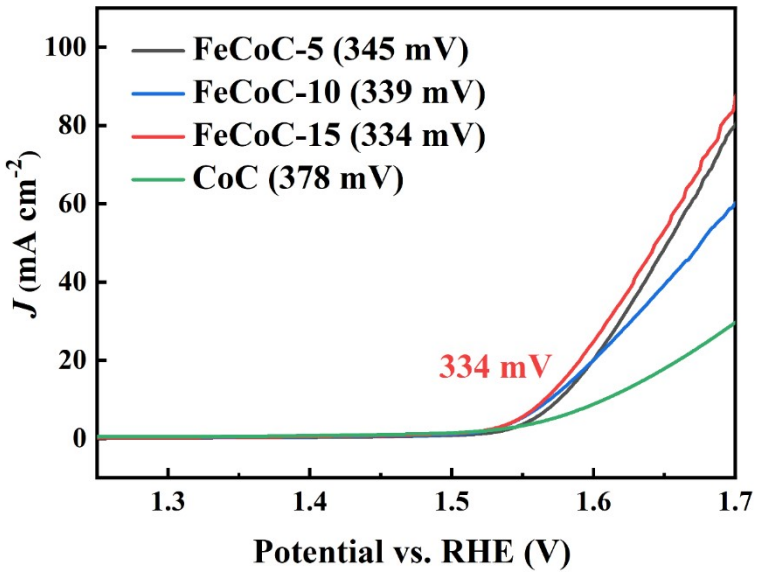

Figure S15. The LSV polarization plots of CoC and FeCoC series.

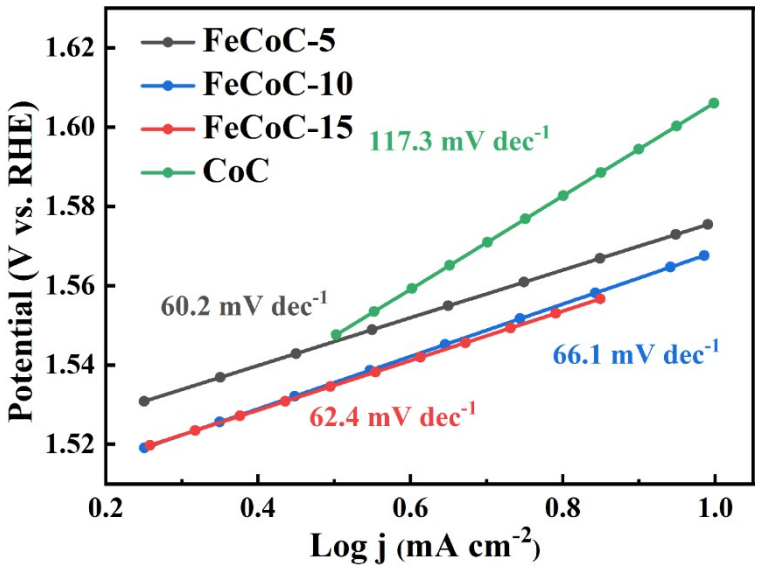

Figure S16. The Tafel plots of CoC and FeCoC series.

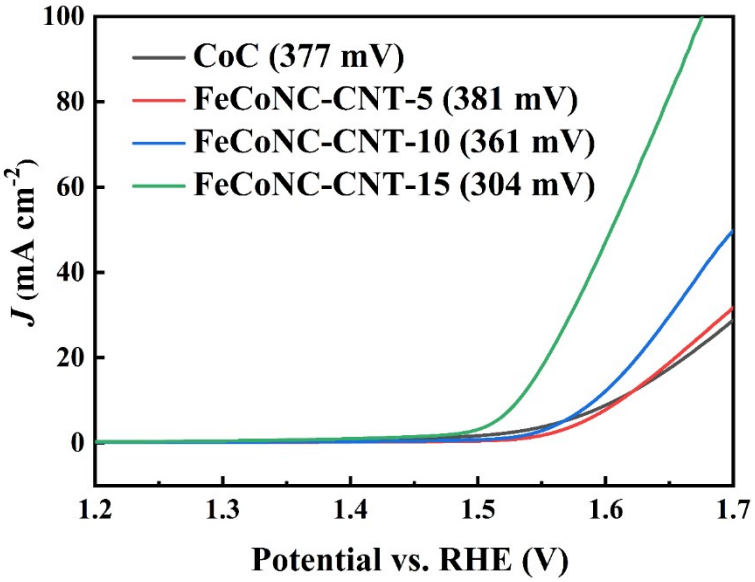

Figure S17. The LSV polarization plots of CoC and FeCoNC-CNT series.

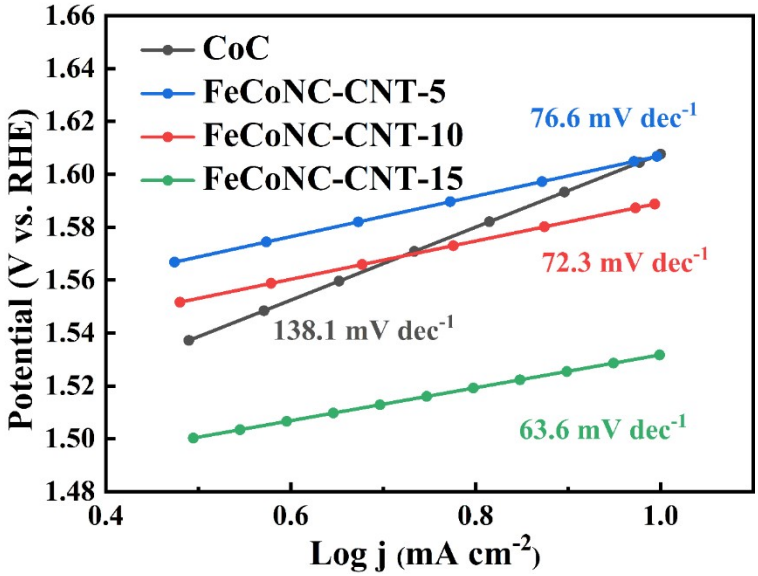

Figure S18. The Tafel plots of CoC and FeCoNC-CNT series.

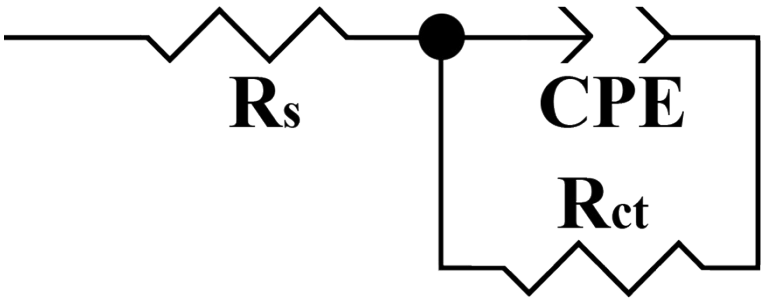

Figure S19. The equivalent circuit of EIS analysis.

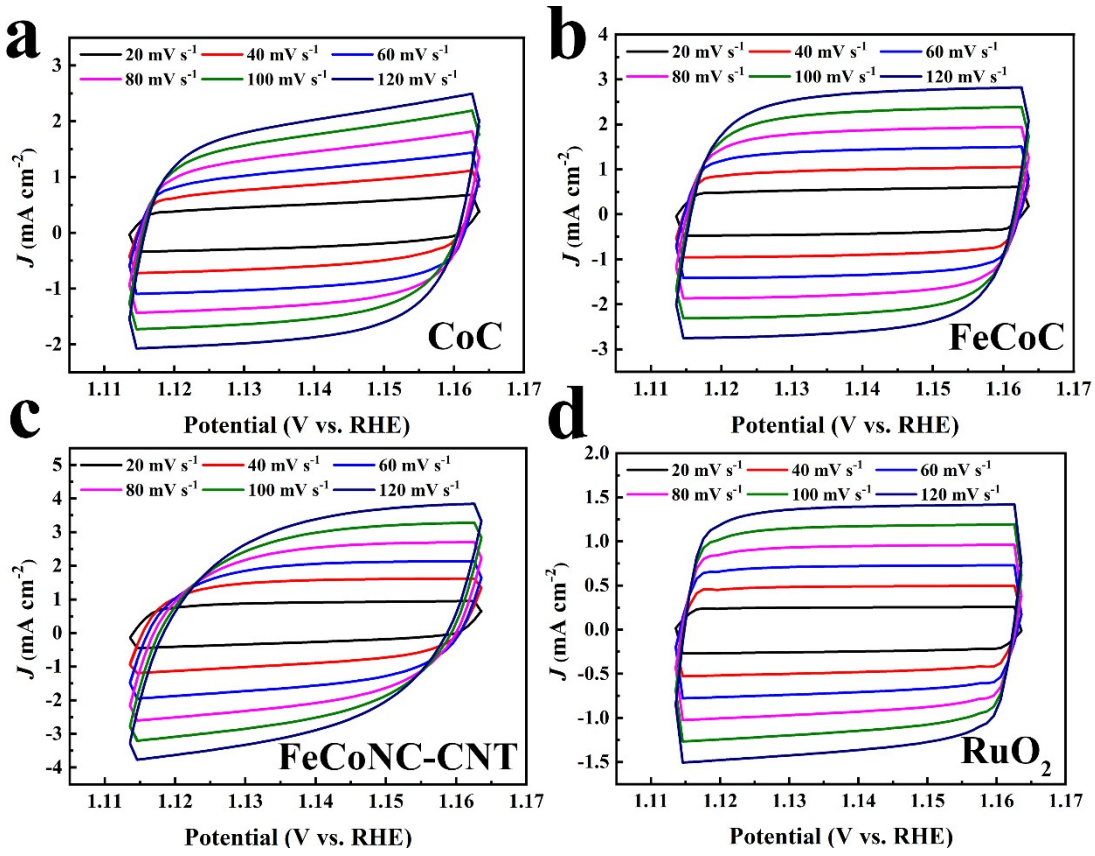

Figure S20. CV curves from 20 to 120 mV s^{-1} for (a) CoC, (b) FeCoC, (c) FeCoNC-CNT, and (d) RuO_2 in 1.0 M KOH.

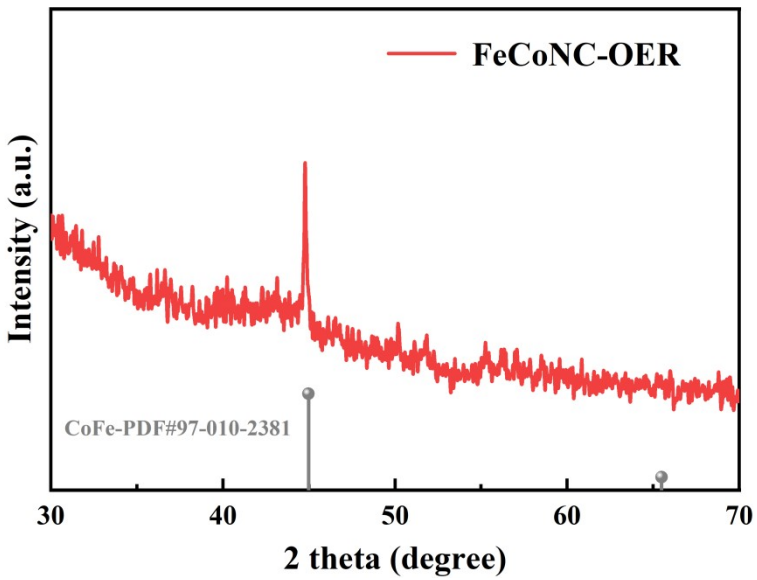

Figure S21. PXRD pattern of FeCoNC-CNT after 60 h CP test.

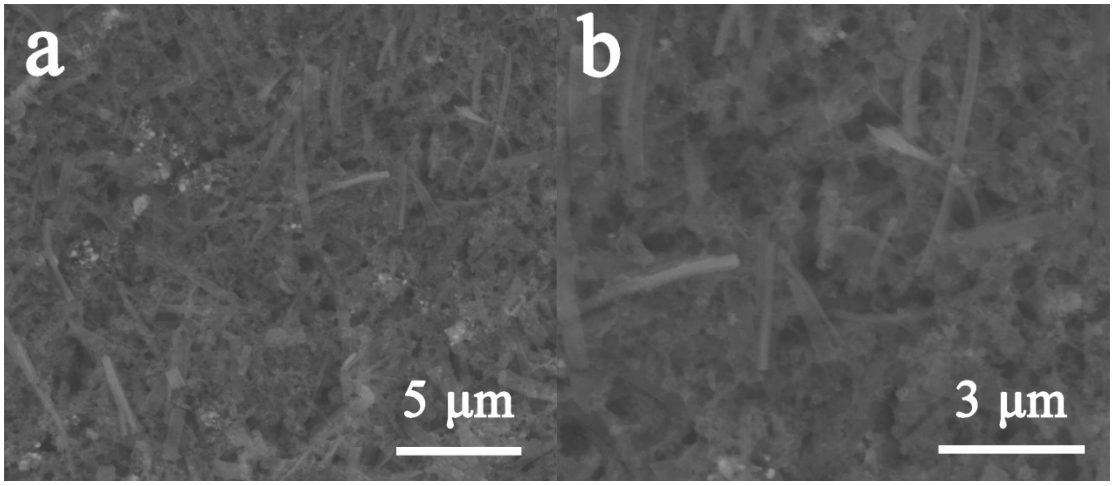

Figure S22. The SEM images of FeCoNC-CNT after the long-term CP test.

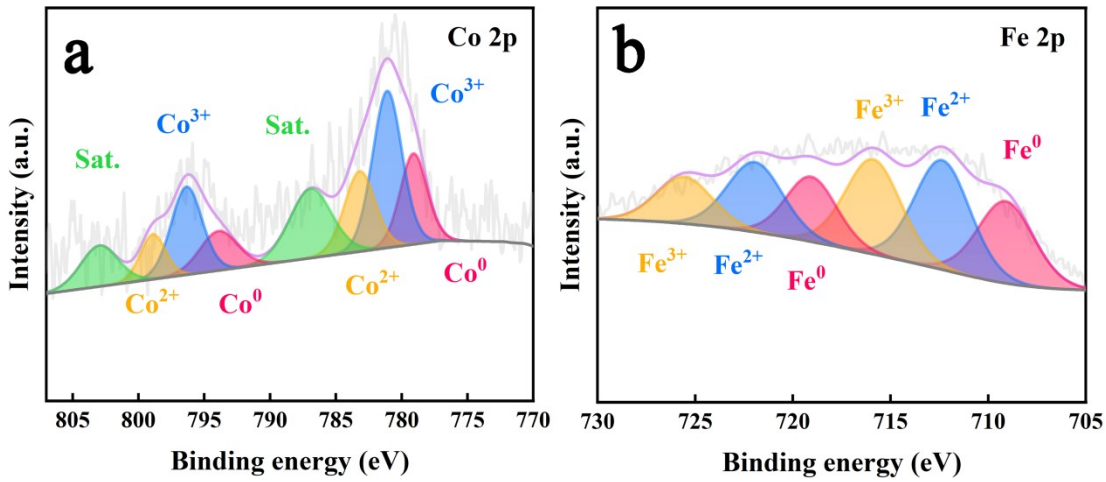

Figure S23. The high-resolution XPS spectra of Co 2p and Fe 2p for FeCoNC-CNT after 60-hour CP test.

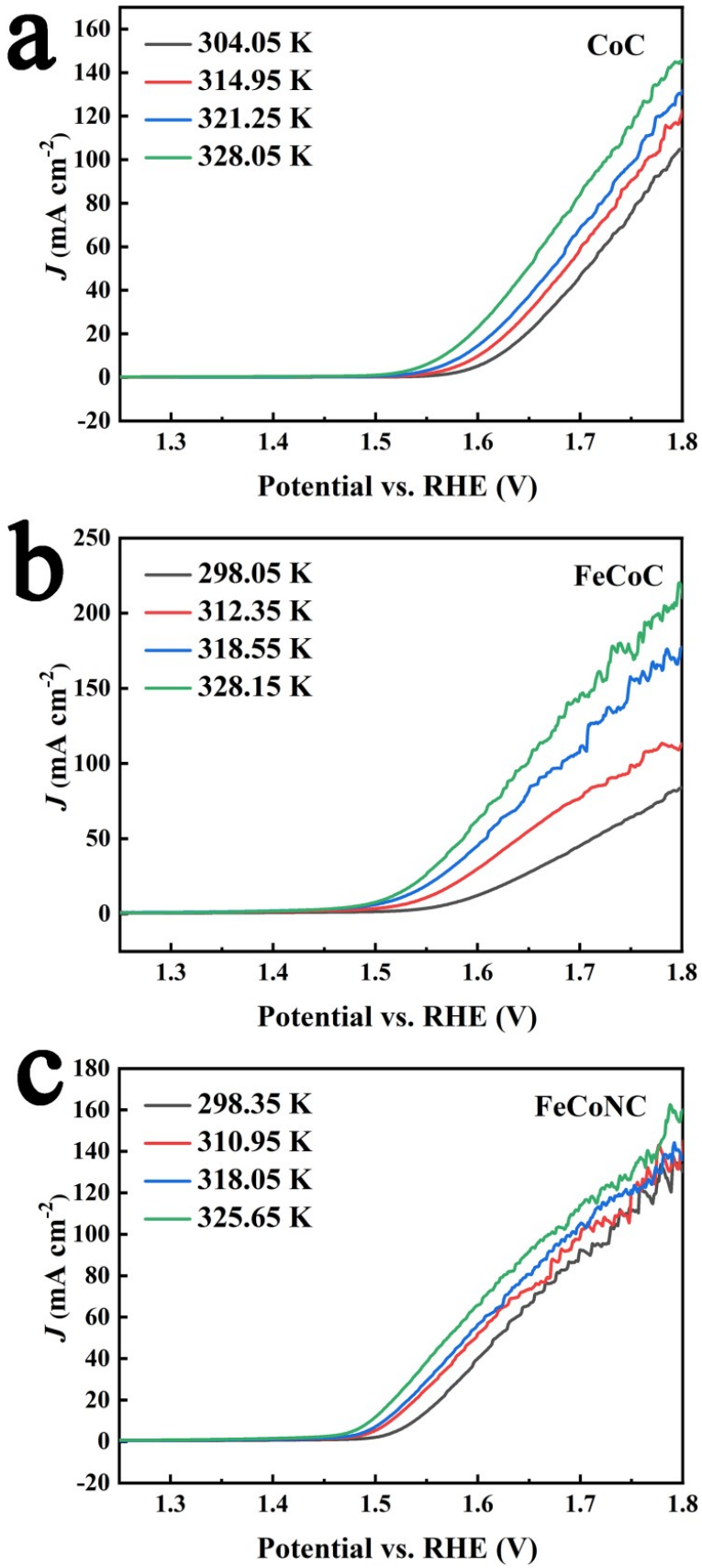

Figure S24. Temperature-dependent LSV curves of (a) CoC, (b) FeCoC, and (c) FeCoNC-CNT with a sweep rate of 5 mV s^{-1}.

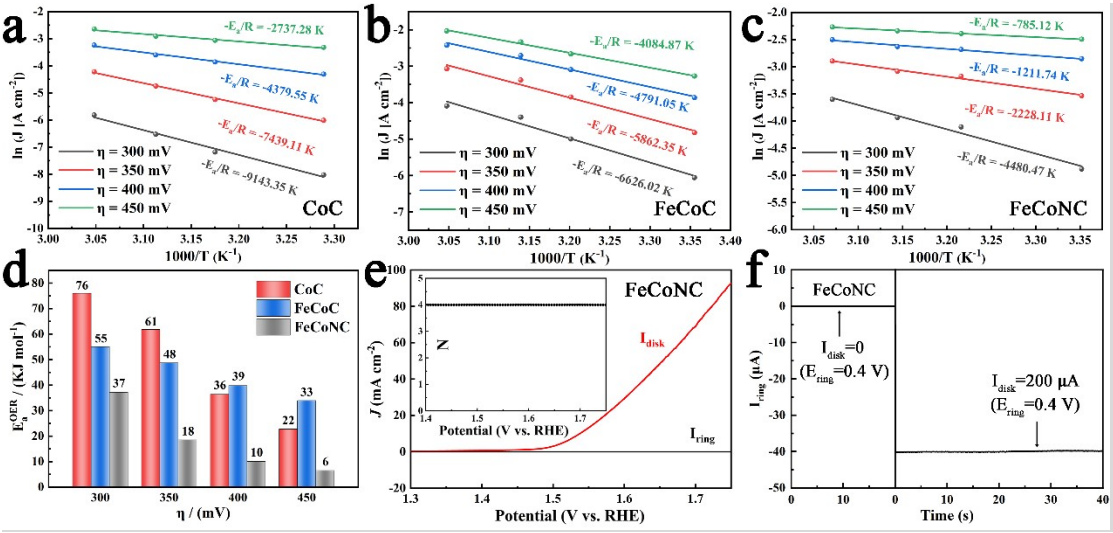

Figure S25. (a-c) Arrhenius plots of CoC, FeCoC, and FeCoNC-CNT at different overpotentials. (d) The calculated E_a values of all three samples. (e) RRDE Voltammogram and its calculated N numbers, and (f) the time-dependent ring current of FeCoNC-CNT.

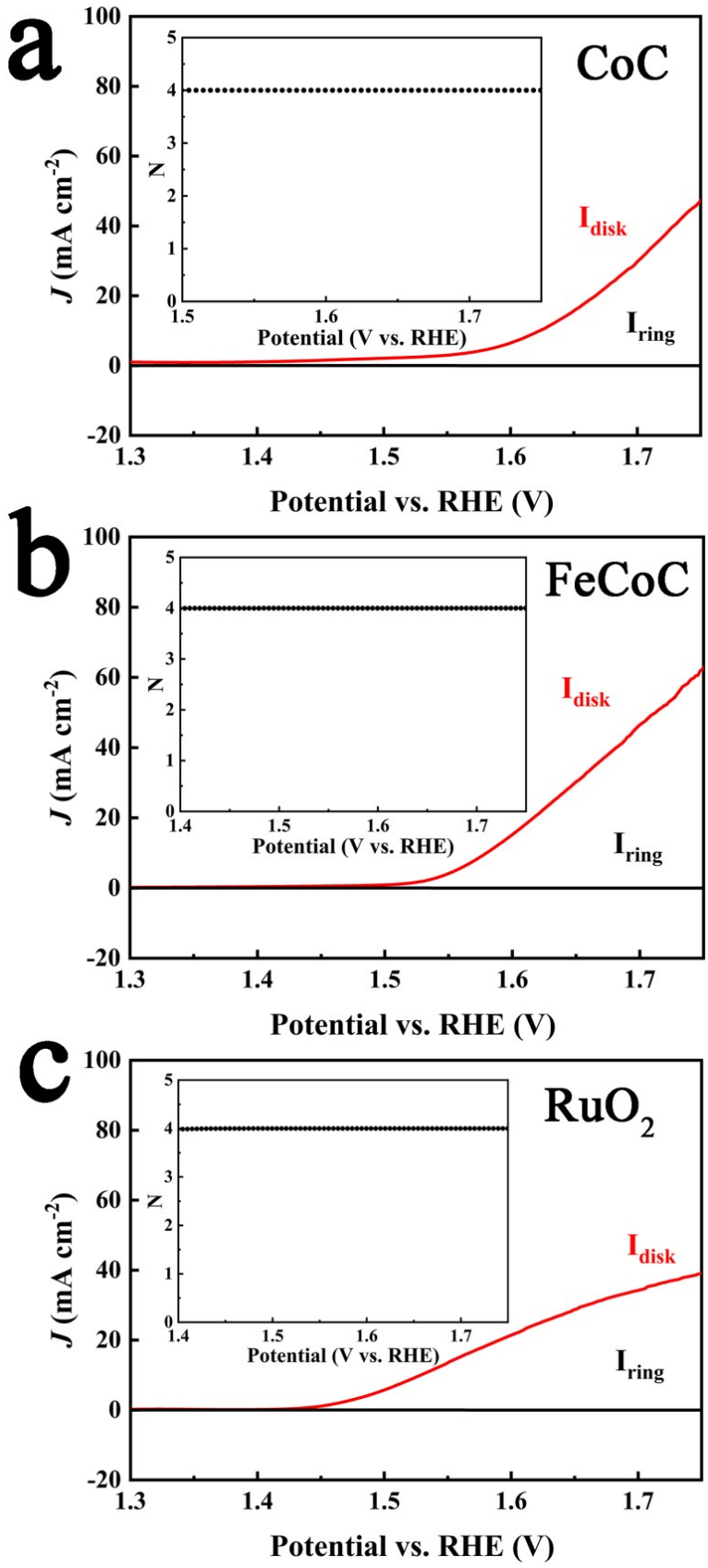

Figure S26. RRDE voltammogram and the calculated N for (a) CoC, (b) FeCoC and (c) RuO_2.

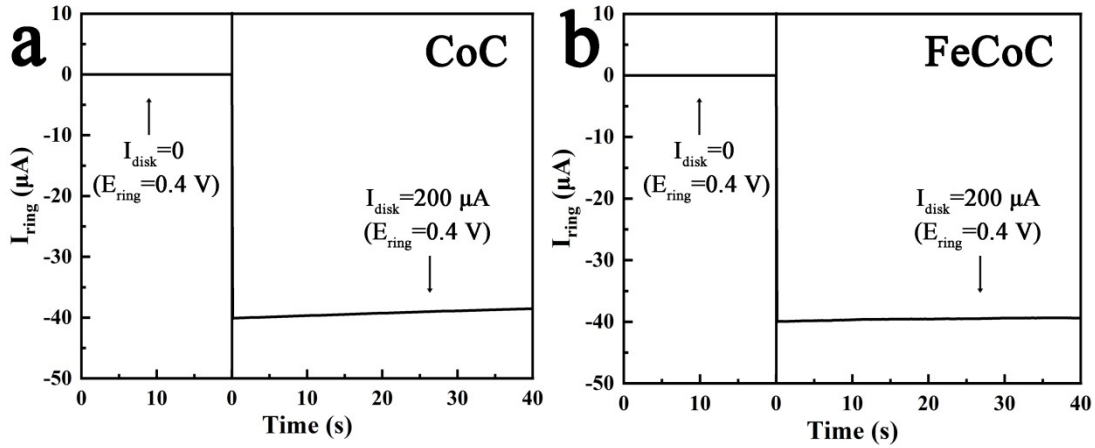

Figure S27. RRDE voltammogram and the time dependent ring current of (a) CoC and (b) FeCoC.

Table S1. Summary of Crystal Data for CoOF-1.

Compound	**CoOF-1**[Ref.1]
Chemical formula	$C_8H_3CoNO_7$
Formula mass	284.1
Crystal system	Tetragonal
Space group	*$I4_122$*
a (Å)	15.327 (3)
b (Å)	15.327 (3)
c (Å)	12.270 (3)
α (°)	90
β(°)	90
γ(°)	90
Unit cell volume (Å^3)	2882.6 (13)
Temperature (K)	296
Z	8
R_1 (I>2σ(I))	0.0310 (1749)
wR (all reflections)	0.0866 (1811)

Ref. 1.[1] (1) Zhong, L.; Ding, J.; Wang, X.; Chai, L.; Li, T.-T.; Su, K.; Hu, Y.; Qian, J.; Huang, S. Structural and Morphological Conversion between Two Co-Based MOFs for Enhanced Water Oxidation. *Inorg. Chem.* **2020**, 59, 2701-2710.

Table S2. Summary of Pore Characteristics of CoC, FeCoC-5/10/15 and FeCoNC-CNT-5/10/15.

Samples	Surface area/m^2 g^{-1} (BET)	Total pore volume[a] /cm^3 g^{-1}	Micropore volume[b] /cm^3 g^{-1}
CoC	71	0.2709	0.0296
FeCoC-5	106	0.2113	0.0471
FeCoC-10	202	0.5759	0.0858
FeCoC-15	278	0.5287	0.1259
FeCoNC-CNT-5	99	0.5338	0.0443
FeCoNC-CNT-10	160	0.5377	0.0708
FeCoNC-CNT-15	323	0.6774	0.1460

a At P/P0=0.99.

b Determined by NLDFT method.

Table S3. The content of Co, Fe in CoC, FeCoC and FeCoNC Series by ICP-MS Measurement.

Samples	Co (w %)	Fe (w %)
CoC	47.23	/
FeCoC-5	37.62	5.03
FeCoC-10	26.14	10.27
FeCoC-15	17.52	14.26
FeCoNC-5	38.54	5.98
FeCoNC-10	25.82	9.64
FeCoNC-15	15.46	13.58

Table S4. Deconvoluted Peak Position of Co 2p in CoC, FeCoC, FeCoNC-CNT.

Sample	Co^0 $2p_{3/2}$	Co^{3+} $2p_{3/2}$	Co^{2+} $2p_{3/2}$	Co^0 $2p_{1/2}$	Co^{3+} $2p_{1/2}$	Co^{2+} $2p_{1/2}$
CoC	778.5 eV	780.1 eV	781.9 eV	793.2 eV	795.1 eV	797.1 eV
FeCoC	779.2 eV	780.8 eV	782.6 eV	793.9 eV	796.8 eV	797.8 eV
FeCoNC-CNT	779.2 eV	780.8 eV	782.6 eV	793.9 eV	796.8 eV	797.8 eV

Table S5. Deconvoluted Peak Position of Fe 2p in FeCoC and FeCoNC-CNT.

Sample	Fe^0 $2p_{3/2}$	Fe^{2+} $2p_{3/2}$	Fe^{3+} $2p_{3/2}$	Fe^0 $2p_{1/2}$	Fe^{2+} $2p_{1/2}$	Fe^{3+} $2p_{1/2}$
FeCoC	709.1 eV	712.1 eV	715.1 eV	719.5 eV	722.1 eV	725.2 eV
FeCoNC-CNT	709.1 eV	712.1 eV	715.1 eV	719.5 eV	722.1 eV	725.2 eV

Table S6. Deconvoluted Peak Position of N 1s in FeCoNC-CNT.

Sample	pyridinic-N	pyrrolic-N	graphitic-N	oxidized-N
FeCoNC-CNT	398.3 eV	399.8 eV	401.3 eV	403.2 eV

Table S7. The Summary of Electrochemical Data of CoC, FeCoC, FeCoNC-CNT and RuO_2.

Samples	Overpotential (mV, η_{10})	Overpotential (mV, η_{50})	Tafel slope (mV dec^{-1})	C_{dl} value (mF cm^{-2})	Charge transfer resistance (Ω)
CoC	370	497	109.2	15.5	3.7
FeCoC	335	393	55.4	21.6	3.6
FeCoNC -CNT	296	343	52.8	25.2	1.2
RuO_2	320	398	57.2	11.3	4.5

Table S8. The Activation Energies of CoC, FeCoC, and FeCoNC-CNT at Different Overpotentials.

Sample	EOER a (300 mV)	EOER a (350 mV)	EOER a (400 mV)	EOER a (450 mV)
CoC	76.02 kJ mol^{-1}	61.85 kJ mol^{-1}	36.41 kJ mol^{-1}	22.76 kJ mol^{-1}
FeCoC	55.09 kJ mol^{-1}	48.74 kJ mol^{-1}	39.83 kJ mol^{-1}	33.96 kJ mol^{-1}
FeCoNC-CNT	37.25 kJ mol^{-1}	18.52 kJ mol^{-1}	10.07 kJ mol^{-1}	6.52 kJ mol^{-1}

Table S9. Comparison of Various OER Electrocatalysts in Alkaline Solution.

Samples	Electrolyte	η_{10} /mV	Tafel slope /mV dec^{-1}	Ref.
FeCoNC-CNT	1.0 M KOH	304	62.3	**This work**
Co_2P/FeCo/MnNP-BCNTs	1.0 M KOH	324	72.5	**Ref**[2]
FeCo/PCNs	1.0 M KOH	344	74.4	**Ref**[3]
FeCo/S-NC	1.0 M KOH	299	127	**Ref**[4]
FeCo-3/NSC	1.0 M KOH	312	96.4	**Ref**[5]
FeCo@BNPCNS-900	1.0 M KOH	339	65.2	**Ref**[6]
CoFe@N-CNTs-800	1.0 M KOH	306	63	**Ref**[7]
FeCo/FeCoP@NMn-CNS-800	1.0 M KOH	325	63.2	**Ref**[8]
FeCo/FeN_2/NHOPC	1.0 M KOH	340	106	**Ref**[9]
FeCo-TA@CMS	1.0 M KOH	380	99	**Ref**[10]
FeCo-LCNT	0.1 M KOH	385	126	**Ref**[11]

References

(1) Zhong, L.; Ding, J.; Wang, X.; Chai, L.; Li, T.-T.; Su, K.; Hu, Y.; Qian, J.; Huang, S. Structural and Morphological Conversion between Two Co-Based MOFs for Enhanced Water Oxidation. *Inorg. Chem.* **2020**, 59, 2701-2710.

(2) Han, Z.; Feng, J.-J.; Yao, Y.-Q.; Wang, Z.-G.; Zhang, L.; Wang, A.-J. Mn, N, P-tridoped bamboo-like carbon nanotubes decorated with ultrafine Co2P/FeCo nanoparticles as bifunctional oxygen electrocatalyst for long-term rechargeable Zn-air battery. *J. Colloid Interface Sci.* **2021**, 590, 330-340.

(3) Lei, Y.; Zhang, F.; Li, G.; Yang, J.; Hu, H.; Shen, Y.; Zhang, X.; Wang, X. FeCo alloy nanoparticles embedded in nitrogen-doped carbon nanospheres as efficient bifunctional electrocatalysts for oxygen reduction and oxygen evolution reaction. *Int. J. Hydrogen Energy* **2024**, 65, 437-444.

(4) Chang, H.; Zhao, L.; Zhao, S.; Liu, Z.-L.; Wang, P.-F.; Xie, Y.; Yi, T.-F. Tuning interface mechanism of FeCo alloy embedded N,S-codoped carbon substrate for rechargeable Zn-air battery. *J. Energy Chem.* **2024**, 93, 400-410.

(5) Chang, S.; Zhang, H.; Zhang, Z. FeCo alloy/N, S dual-doped carbon composite as a high-performance bifunctional catalyst in an advanced rechargeable zinc-air battery. *J. Energy Chem.* **2021**, 56, 64-71.

(6) Xiao, L.; Wang, Y.; Fu, T.; Liu, Q.; Guo, F.; Zhang, Y.; Li, M.; Bo, X.; Liu, T. Facile synthesis of ultrafine iron-cobalt (FeCo) nanocrystallite-embedded boron/nitrogen-codoped porous carbon nanosheets: Accelerated water splitting catalysts. *J. Colloid Interface Sci.* **2024**, 654, 150-163.

(7) Guo, P.; Wu, R.; Fei, B.; Liu, J.; Liu, D.; Yan, X.; Pan, H. Multifunctional bayberry-like composites consisting of CoFe encapsulated by carbon nanotubes for overall water splitting and zinc–air batteries. *J. Mater. Chem. A* **2021**, 9, 21741-21749.

(8) Chen, Y.-P.; Lin, S.-Y.; Sun, R.-M.; Wang, A.-J.; Zhang, L.; Ma, X.; Feng, J.-J. FeCo/FeCoP encapsulated in N, Mn-codoped three-dimensional fluffy porous carbon nanostructures as highly efficient bifunctional electrocatalyst with multi-components

synergistic catalysis for ultra-stable rechargeable Zn-air batteries. *J. Colloid Interface Sci.* **2022**, 605, 451-462.

(9) Wang, Y.; Qiao, M.; Mamat, X. An advantage combined strategy for preparing bi-functional electrocatalyst in rechargeable zinc-air batteries. *Chem. Eng. J.* **2020**, 402, 126214.

(10) Liu, H.; Yang, D.-H.; Wang, X.-Y.; Zhang, J.; Han, B.-H. N-doped graphitic carbon shell-encapsulated FeCo alloy derived from metal–polyphenol network and melamine sponge for oxygen reduction, oxygen evolution, and hydrogen evolution reactions in alkaline media. *J. Colloid Interface Sci.* **2021**, 581, 362-373.

(11) Deng, Y.; Zheng, J.; Liu, B.; Liu, Y.; Li, H.; Yang, M. Schiff-base polymer derived ultralong FeCo/N-doped carbon nanotubes as bifunctional oxygen electrocatalyst for liquid and flexible all-solid-state rechargeable zinc–air batteries. *Carbon* **2023**, 210, 118000.